Supplementary Information for

The mechanism of charge transfer between quantum dots and redox molecules

Yan B. Vogel,[*,†] Willemijn Boeije,[†,1] Lotte van Steekelenburg,[†,1] Demi Vollebregt,[†] Reinout Ubbink,[†] Hua Chen,[†] Ali Tayefeh Younesi,[‡] Ronald Ulbricht,[‡] Wolter Jager,[†] Ferdinand Grozema,[†] Arjan Houtepen[†]

[†]*Department of Chemical Engineering, Delft University of Technology, Van der Maasweg 9, 2629 HZ Delft, The Netherlands*

[‡]*Max Planck Institute for Polymer Research, Ackermannweg 10, 55128, Mainz, Germany*

[1]*These authors contributed equally*

Contents

S0: Materials and methods

Materials. All materials were purchased from Sigma-Aldrich unless otherwise stated. For the synthesis of PbS QDs we used lead (II) oxide (PbO, 99.999%), octadecene (ODE, 90%), bis(trimethylsilyl) sulfide (TMS, synthesis grade), and oleic acid (OA, extra pure, Thermo Fisher Scientific). For the synthesis of the ferrocene derivatives, we used 6-bromohexanoylchloride (97%), chloroacetyl chloride (98%), aluminum chloride ($AlCl_3$, 98%, anhydrous), dichloromethane (DCM, ⩾99.8%, anhydrous), ferrocene (Fc, 98%), hexamethyldisilathiane ($(TMS)_2S$, synthesis grade), tetrahydrofuran (THF, 99.9%, anhydrous), and tetra-n-butylammonium fluoride (TBAF, 1.0 M solution in THF). For the ferrocene derivatives workup we used magnesium sulfate ($MgSO_4$), and silica gel (siliaflash, 40-63 µm, Silicycle), and technical grade dichloromethane, petroleum ether, and ethyl acetate. All NMR were performed in deuterated chloroform (+0.03% TMS, 99,80%, Eurisotop). The QDs were dispersed in tetrachloroethylene (TCE, ⩾99%, anhydrous) for further analysis, except for NMR.

Synthesis of PbS QDs. PbS QDs were synthesized following a previously described procedure.[50] In a typical synthesis, lead(II) oxide (90 mg) was dissolved in OA (0.25 mL) and ODE (3 mL) by heating under vacuum to 100 °C for 1 h. The temperature was then set to the desired temperature (e.g., 150 °C), and a solution of TMS (42 µL) in ODE (0.75 mL) was injected under a nitrogen atmosphere. The heating mantle was lowered away from direct contact with the reaction flask immediately after injection of the TMS solution and allowed to cool to room temperature. The PbS QD size was adjusted by modifying the OA/Pb/S ratio (from 4:2:1 to 80:2:1) and temperature (115–150 °C). The PbS QDs were isolated from the reaction mixture by adding acetone until the solution became turbid, centrifuged, the supernatant removed, and the QDs redispersed in 8 mL of tetrachloroethylene. The QD dispersion was stored at room temperature.

Synthesis of ferrocene-ethan-2-one-1-thiol ($FcOC_2SH$). The synthesis of $FcOC_2SH$ consisted in a Friedel-Craft acylation to obtain 2-ferrocene-ethan-2-one-1-chloride ($FcOC_2Cl$) which has been previously described,[71] followed by a thiolation to obtain the final product ($FcOC_2SH$). **Synthesis of $FcOC_2Cl$.** $FcOC_2Cl$ was synthesized following a previously described procedure.[71] Ferrocene (15 g, 81 mmol) and DCM (100 mL) were added to a 250 mL three-neck round-bottom flask under argon and cooled to -15 ºC. Chloroacetyl chloride (6g, 53 mmol) was added to the flask. Anhydrous $AlCl_3$ (7.15 g, 54 mmol) was added slowly over a period of 4h, keeping it stirring, at -15 ºC, and under argon. After addition, the reaction was allowed to reach room temperature and kept stirring overnight. The reaction was quenched with ice and extracted with DCM and water. The organic layer was dried by magnesium sulfate and the solvent was evaporated by a rotary evaporator. The obtained solid was purified by column chromatography with an eluent of hexane/DCM (2:1), and the solvent was evaporated by a rotary evaporator to obtain $FcOC_2Cl$ (5.5 g, 21 mmol, 40% yield). ^1H NMR (399.7 MHz, Chloroform-d): δ=4.8 (m, 2H),

4.6 (m, 2H), 4.4 (s, 2H), 4.2 (s, 4H). ^{13}C NMR (100 MHz, Chloroform-d): δ=195.3, 75.9, 73.0, 70.2, 69.5, 46.0ppm. **Synthesis of $FcOC_2SH$.** A 100 mL round bottom flask was charged with $FcOC_2Cl$ (2.75 g, 10 mmol), and THF (20 mL) was added under argon. $(TMS)_2S$ (3.16 mL, 15 mmol) was added under stirring and cooled to -15 ºC. A TBAF solution (15 mL, 15 mmol, 1 M in THF) was added dropwise to the solution, allowed to reach room temperature, and let react for 1 hr at room temperature. The reaction was quenched with ice water and diluted in dichloromethane. It was washed three times with water, dried using $MgSO_4$ and the solvent was evaporated by a rotary evaporator. The obtained solid was purified by column chromatography with an eluent of petroleum ether/ethyl acetate (5:1), and the solvent was evaporated by a rotary evaporator to obtain $FcOC_2SH$ (1.1 g, 4.2 mmol, 42% yield). ^{1}H NMR (399.7 MHz, Chloroform-d): δ= 4.8 (dt, J=5.6, 2.0 Hz, 2H), 4.5 (dt, J=6.2, 2.0 Hz, 2H), 4.2 (d, J=4.9 Hz, 5H), 3.7 (s, 2H). ^{13}C NMR (100 MHz, Chloroform-d): δ=198.69, 72.84, 70.04, 69.78, 38.26 ppm.

Synthesis of ferrocene-hexan-6-one-1-thiol ($FcOC_6SH$). $FcOC_6SH$ was synthesized following a previously described procedure.[72] This consisted in a Friedel-Crafts acylation to obtain ferrocene-hexanone-1-bromide ($FcOC_6Br$) followed by a thiolation to obtain the final product. **Synthesis of $FcOC_6Br$.** A 50 mL round-bottom flask was charged with ferrocene (5.50 g, 35.2mmol), DCM (15mL) and $AlCl_3$ (2.19 g, 14.0 mmol) and put under argon at 0 ◦C under stirring. 6-bromohexanoylchloride (1.96 mL,12.7 mmol) dissolved in DCM (5 mL) was added dropwise. After 2 hours the reaction was quenched with water, diluted with DCM, and washed twice with water. The organic layer was dried over MgSO4, and the solvent removed by rotary evaporation. The obtained solid was purified via column chromatography with hexane as eluent to elute unreacted Fc. Gradually, ethyl acetate was added to the eluent to obtain the product (2.76 g, 7.59 mmol, 60% yield). ^{1}H NMR (399.7 MHz, Chloroform-d): δ=4.77 (t, J=1.9 Hz, 2H), 4.48 (t, J=1.9 Hz, 2H), 4.18 (s, 3H), 3.43 (t, J=6.8 Hz, 2H), 2.71(t, J=7.4 Hz, 2H), 1.90 (p, J=14.9, 7.8, 7.4 Hz, 2H), 1.73 (p, 2H), 1.53 (m, 2H). ^{13}C NMR (100 MHz, Chloroform-d): δ=204.3, 79.0, 72.2, 69.7, 69.3, 39.4, 33.7, 32.6, 28.0, 23.6 ppm. **Synthesis of $FcOC_6SH$.** A 25 mL round-bottom flask was charged with $FcOC_6Br$ (930 mg, 2.56 mmol), put under argon, added (TMS)2S (654 µL, 3.07 mmol) and THF (5 mL), and cooled to 0 ◦C under stirring. A TBAF solution (2.82 mL, 2.82 mmol, 1 M in THF) was added dropwise. After 70 minutes the reaction was quenched with ice water, diluted with diethyl ether and washed five times with water. The organic layer was dried over $MgSO_4$, and the solvent was removed by rotary evaporation. The obtained solid was purified by column chromatography with an eluent of hexane/ethyl acetate (4:1) to separate residual Fc and a dithiol impurity from the desired product. This resulted in $FcOC_6SH$ (406 mg,1.28 mmol, 50% yield). ^{1}H NMR (399.7 MHz, Chloroform-d): δ=4.78 (t, J=1.7 Hz, 2H), 4.49 (t, J=1.7 Hz, 2H), 4.19 (s, 5H), 2.71 (t, J=7.3 Hz, 2H), 2.56 (q, J=7.4 Hz, 2H), 1.71 (m, 2H), 1.49 (m, 1H), 1.36 (t, J=7.8, 1.4 Hz, 1H). ^{13}C NMR (100 MHz, Chloroform-d): δ=204.3, 79.1, 72.1, 69.7, 69.3, 39.4, 33.8, 28.2, 24.5, 23.9 ppm.

Anchoring redox ligands onto PbS QDs. Anchoring $FcOC_2SH$ or $FcOC_6SH$ onto PbS QDs was performed by mixing 500 µL of the obtained PbS solution with 500 µL of chloroform and 1 mL of a solution of $FcOC_2SH$ or $FcOC_6SH$ in chloroform at concentrations between 100 mM and 5 mM. This solution was left stirring overnight at room temperature in a glovebox. The ligand exchanged particles were purified by washing them with acetone (12 mL) and tetrachloroethylene (1 mL) three times to discard unreacted $FcOC_2SH$ or $FcOC_6SH$. The precipitate was dried under vacuum for 10 minutes and redissolved in tetrachloroethylene, except for the NMR measurements where the precipitate was redissolved in $CDCl_3$.

X-ray photoelectron spectroscopy. The XPS measurements were performed under UHV ($<2 \times 10^{-7}$ mbar) on a Thermo Fisher K-Alpha equipped with an Al Kα source. The XPS samples were prepared by drop casting 20 µL of the QD solution onto a cleaned ITO on glass substrate. The ITO substrate was cleaned by thoroughly rinsing it with acetone and isopropanol and put for 20 minutes in a UV/O_3 chamber.

Transmission electron microscopy. Transmission electron microscopy images were acquired using a JEOL JEM1400 transmission electron microscope operating at 120 keV. The TEM samples were prepared by drop casting a diluted QD solution onto the carbon-coated copper TEM grids. Size distributions were calculated using the software ImageJ from at least 100 QDs.

Nuclear magnetic resonance spectroscopy. Solution ^{1}H and ^{13}C NMR spectra were collected with a 400 MHz Agilent spectrometer (^{1}H :399.7 MHz; ^{13}C 100 MHz). All samples were prepared in Chloroform-d3 and referenced to the residual protons or 13C nuclei in the NMR solvent relative to $(CH_3)_4Si$ (δ [ppm]); ^{1}H: Chloroform-d δ =7.26 ppm.

Transient absorption spectroscopy. The QD samples were prepared by diluting them in tetrachloroethylene to obtain an absorbance of ca. 0.1 O.D. The measurement was performed in a 2 mm pathlength cuvette under vigorous stirring to avoid charging. Laser pulses of 180 fs were generated in a Yb:KGW oscillator (Light Conversion, Pharos SP) at 1028 nm and amplified. A small fraction of the 1028 nm fundamental beam was split off to generate the broadband probe spectrum in a sapphire crystal. The probe pulse was delayed up to 3 ns using an automated delay stage. Most of the 1028 nm fundamental beam was used as a pump pulse after nonlinear frequency mixing in an OPA and second harmonics module (Light Conversion, Orpheus) to achieve wavelengths of 310–1500 nm. The pump and probe pulses overlap on the sample position under an angle of ~8°, after which the pump pulse is dumped and the probe light is led to a detector suitable for the probe spectrum selected (Ultrafast Systems, Helios). All shown data is corrected for dispersion by fitting a polynomial function to the solvent response.

Absorption spectroscopy. Steady-state absorption spectra of PbS QDs were recorded using a PerkinElmer Lambda 1050 UV/vis/NIR spectrophotometer.

Photoluminescence spectroscopy. The QD samples were prepared by diluting them in tetrachloroethylene to obtain an absorbance of ca. 0.1 O.D. An Edinburgh Instruments FLS980 spectrofluorometer with double grating monochromators for both excitation and emission paths and a 450 W xenon lamp as an excitation source were used. The PLQY was measured using an Edinburgh Instruments FLS980 spectrometer with a calibrated integrating sphere. The emission was recorded between 650 nm to 1700 nm, and the samples were excited at 700 nm.

Time resolved photoluminescence. The QD samples were prepared by diluting them in tetrachloroethylene to obtain an absorbance of ca. 0.1 O.D. An Edinburgh Instruments Lifespec TCSPC with a 700 nm pulsed laser was used for recording the PL decay traces at the PL emission peak.

S1: Theoretical considerations to develop the experimental model

We developed an experimental model taking into consideration the parameters described within the Marcus theory. Although, *equation (1)* contains all the terms that govern charge transfer, one must also consider the dependences of the parameters H_{QDA}, λ, and ΔG^0, which we describe in this section.

Electronic coupling (H_{AD})

In the limit of weak coupling, H_{QDA} decays exponentially with the distance (d) between QD and A:

$$H_{DA} = H^0_{DA} \exp\left[-\beta d / 2\right] \quad \text{(S1)}$$

Where H^0_{QDA} is the electronic coupling pre-factor and β is the tunneling decay.

Reorganization energy (λ)

λ can be separated into the inner (λ_i) and outer (λ_o) reorganization energy, which represent the contributions from the QDA species and from the solvent, respectively:

$$\lambda = \lambda_i + \lambda_o \quad \text{(S2)}$$

λ_i depends on the difference of all the vibrational modes between QDA and QD^-A^+ and is usually computed using density functional theory. λ_i can be approximated to be the sum from the ferrocene molecule and the QD:

$$\lambda_i = \lambda_{i,Fc} + \lambda_{i,QD} \quad \text{(S3)}$$

The inner reorganization energy for ferrocene is reported to be 15 meV.[1] The inner reorganization energy for PbS QD is a function of diameter. For the diameters considered here, 2.5 nm to 5.7 nm (Figure S2 and S3), this value is reported to be around 25 meV.[2] Therefore, we estimate λ_i = 40 meV.

λ_o can be computed assuming a solvent as a classical dielectric continuum, and QD and A as spheres of radius r_{QD} *and* r_A, respectively:

$$\lambda_o = \frac{e^2}{4\pi\varepsilon_0}\left(\frac{1}{2r_{QD}} + \frac{1}{2r_A} - \frac{1}{d}\right)\left(\frac{1}{\varepsilon_{op}} - \frac{1}{\varepsilon_s}\right) \quad \text{(S4)}$$

Where ε_s and ε_{op} are the static and optical relative permittivity, respectively, and the other parameters have their usual meaning.

We use tetrachloroethylene as a solvent with a static dielectric constant of 2.3.[3] The optical dielectric constant of 2.2 was calculated from the reported refractive index of 1.5057,[3] using the approximation $\varepsilon_{op} = n^2$. The PbS QD diameter investigated here varies between 2.5 nm and 5.7 nm (Figure S2 and S3), and we use a diameter of 4 Å for ferrocene.[4] The distance between QD and A was estimated to be 4.5 Å from the linker length. This gives λ_o = 20 meV.

Hence, the total reorganization energy is 60 meV. We recognize that this value of λ carries some uncertainty as it relies on the set of approximations described above, but we believe it should not differ more than 100 meV at most. For instance, if we vary the QD-A distance between zero and infinite λ ranges from 40 to 80 meV (equation S4). And if we take $1/\varepsilon_{op} - 1/\varepsilon_s$ to be slightly higher (such as if ε_{op} and ε_s are 2.1 and 2.4, respectively) λ becomes 120 meV (equation S4).

Free energy of charge transfer between QD and A (*ΔG*)

Finally, we consider ΔG^0 for both CS and CR, which is given by (see Section S2 for a full derivation):

$$\Delta G_{CS} = E_{A/A+} - E_{VB} \quad \text{(S5)}$$

$$\Delta G_{CR} = E_{CB} - E_{A/A+} \quad \text{(S6)}$$

Where $E_{A/A+}$ is the reduction potential of the molecular acceptor, and E_{VB} and E_{CB} are the valence and conduction band, respectively.

Relationship between rates (*Γ*), pseudo first-order rate constants (*k'*) and rate constants (*k*)

Equation (1) contains the rate constant, but experimentally we measure the CS and CR pseudo first order rate constants (k'_{CS} and k'_{CR}, respectively), related to their respective rate constants (k_{CS} *and* k_{CR}) and rates (Γ_{CS} *and* Γ_{CR}) through:

$$k'_{CS} = k_{CS}[A] \quad \text{(S7)}$$

$$k'_{CR} = k_{CR}[A^+] \quad \text{(S8)}$$

$$\Gamma_{CS} = k_{CS} < N > [A] \quad \text{(S9)}$$

$$\Gamma_{CR} = k_{CR} < N > [A^+] \quad \text{(S10)}$$

With *<N>, [A]* and *[A⁺]* being the number of excitons, acceptors and oxidized acceptors per QD, respectively.

S2: Derivation of the free energy of charge separation and recombination

ΔG^0 is given by the difference in free energy of the initial and final states. For this study, we need to consider ΔG^0 for both CS and CR. For CS the initial state is the excited QD (QD*A), and the final state is the charge separated state (QD^+A^-). The free energy of QD*A is:

$$E_{CS,i} = E_{1Se} + E_{1Sh} + E_{eh} + E_A \quad \text{(S11)}$$

Where E_{1Se} and E_{1Sh} are the electron and hole energies, E_{eh} the electron-hole binding energy, and E_A the energy of the hole acceptor molecule.

After hole transfer from the QD to the molecular acceptor, the free energy of the CS final state QD^+A^- is:

$$E_{CS,f} = E_{1Se} + E_{CS} + E_{c(e)} + E_{c(h)} + E_{A+} \quad \text{(S12)}$$

Where E_{CS} is the electron-hole binding energy in the CS state, $E_{c(e)}$ is the charging energy of putting one electron in the QD, $E_{c(h)}$ is the charging energy of putting one hole in the molecule, and E_{A+} is the energy of the oxidized acceptor molecule.

The total free energy of CS is then: arranging

$$\Delta G^0_{CS} = (E_{1Se} + E_{1Sh} + E_{eh} + E_A) - (E_{1Se} + E_{CS} + E_{c(e)} + E_{c(h)} + E_{A+}) \quad \text{(S13)}$$

Arranging terms:

$$\Delta G^0_{CS} = (E_{A+} - E_A + E_{c(h)}) + (E_{eh} - E_{c(e)} - E_{CS}) + (E_{1Se} - E_{1Se}) + E_{1Sh} \quad \text{(S14)}$$

Noticing that $E_{A/A+} = E_{A+} - E_A + E_{c(h)}$ is the free energy change for oxidizing the molecule, and that $(E_{eh} - E_{c(e)} - E_{CS}) <<< (E_{A/A+} + E_{1Sh})$, we obtain:

$$\Delta G^0_{CS} = E_{A/A+} - E_{1Sh} \quad \text{(S15)}$$

Similarly, the free energy of CR is:

$$\Delta G^0_{CR} = E_{1Se} - E_{A/A+} \quad \text{(S16)}$$

Therefore, to determine ΔG^0 we need to determine $E_{A/A+}$, E_{1Sh} and E_{1Se}.

S3: PbS synthesis and characterization

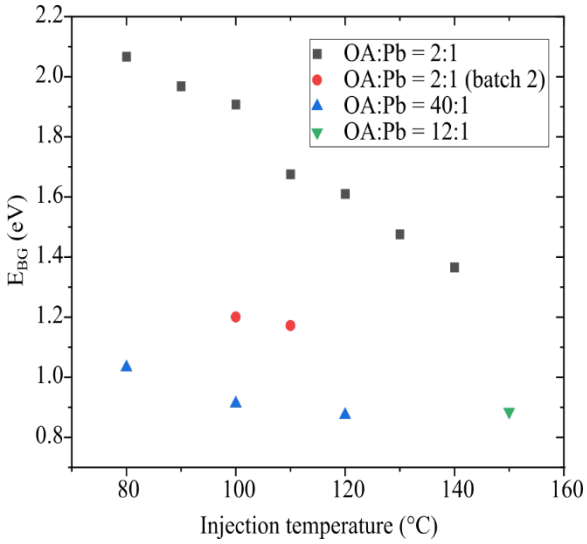

Figure S1. Synthesis of PbS QDs with different bandgap energies. Bandgap energy of PbS as a function of the injection temperature during synthesis for oleic acid to Pb ratios (OA:Pb) of 2:1 (black squares), 12:1 (green triangle) and 40:1 (blue triangles). Also shown oleic acid from a different batch (red circles) with OA:Pb of 2:1.

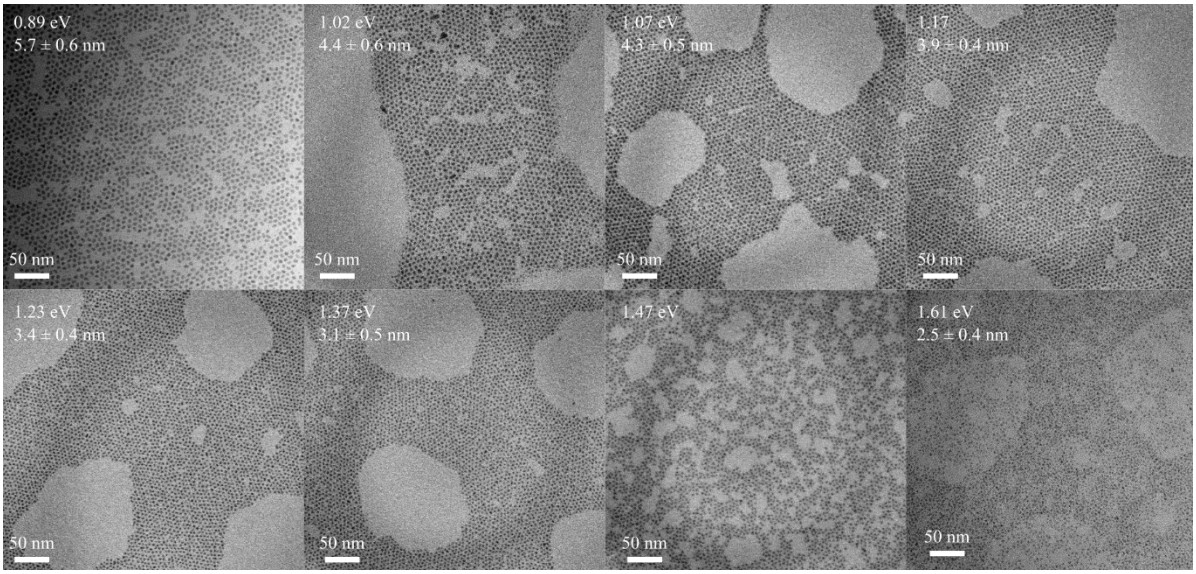

Figure S2. Transmission electron microscopy images of PbS QDs with increasing bandgap energy. The bandgap energy determined by steady-state absorption spectroscopy (Figure 2B) and the QD average diameter and standard deviation determined by TEM are shown as an inset on top of each image.

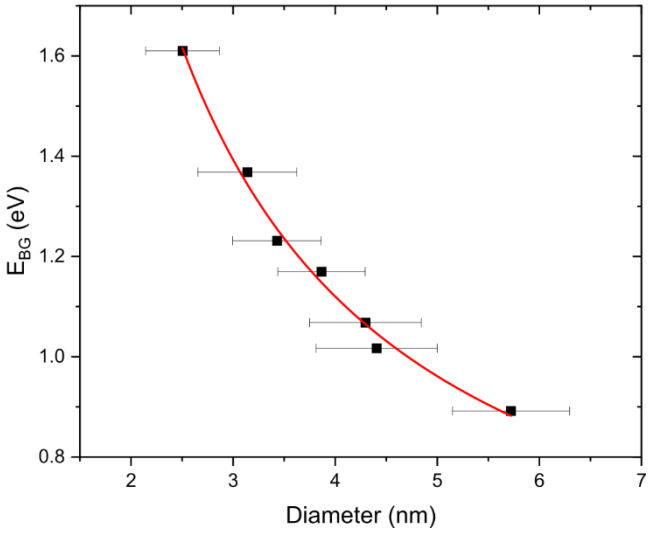

Figure S3. Bandgap energy as a function of the PbS QD average diameter. Bars represent one standard deviation. The diameters were determined from the TEM images (Figure S2) by measuring 100 QDs and the bandgap energy from the $1S_e1S_h$ absorption peak (Figure 2B). A fit to the data (red line) yields the following result: $E_{BG} = 0.41 + \frac{1.36}{d^2} + \frac{2.49}{d}$, with a correlation coefficient of 0.9999.

S4: PbS-$FcOC_2SH$ characterization

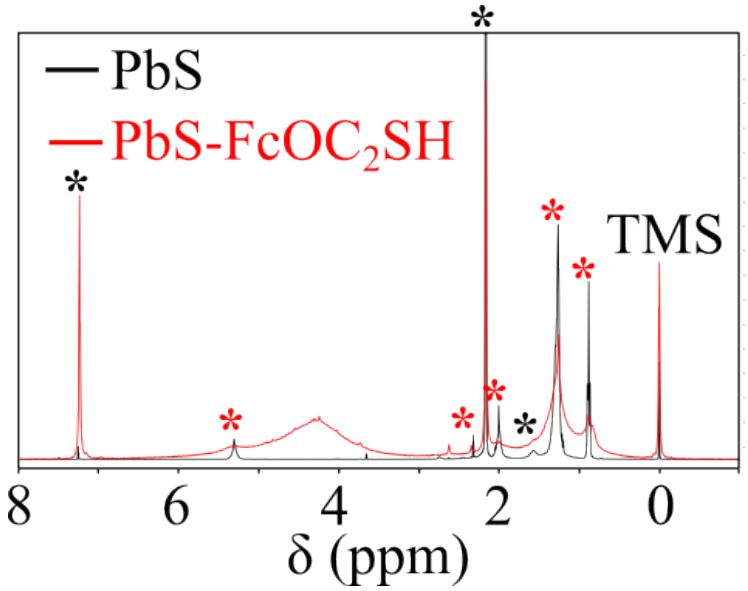

Figure S4. ^1H NMR of PbS with their native oleate ligands (black line) and PbS-$FcOC_2SH$ QDs (red line) in $CDCl_3$. Solvent peaks are indicated with black asterisks and oleate peaks with red asterisks.

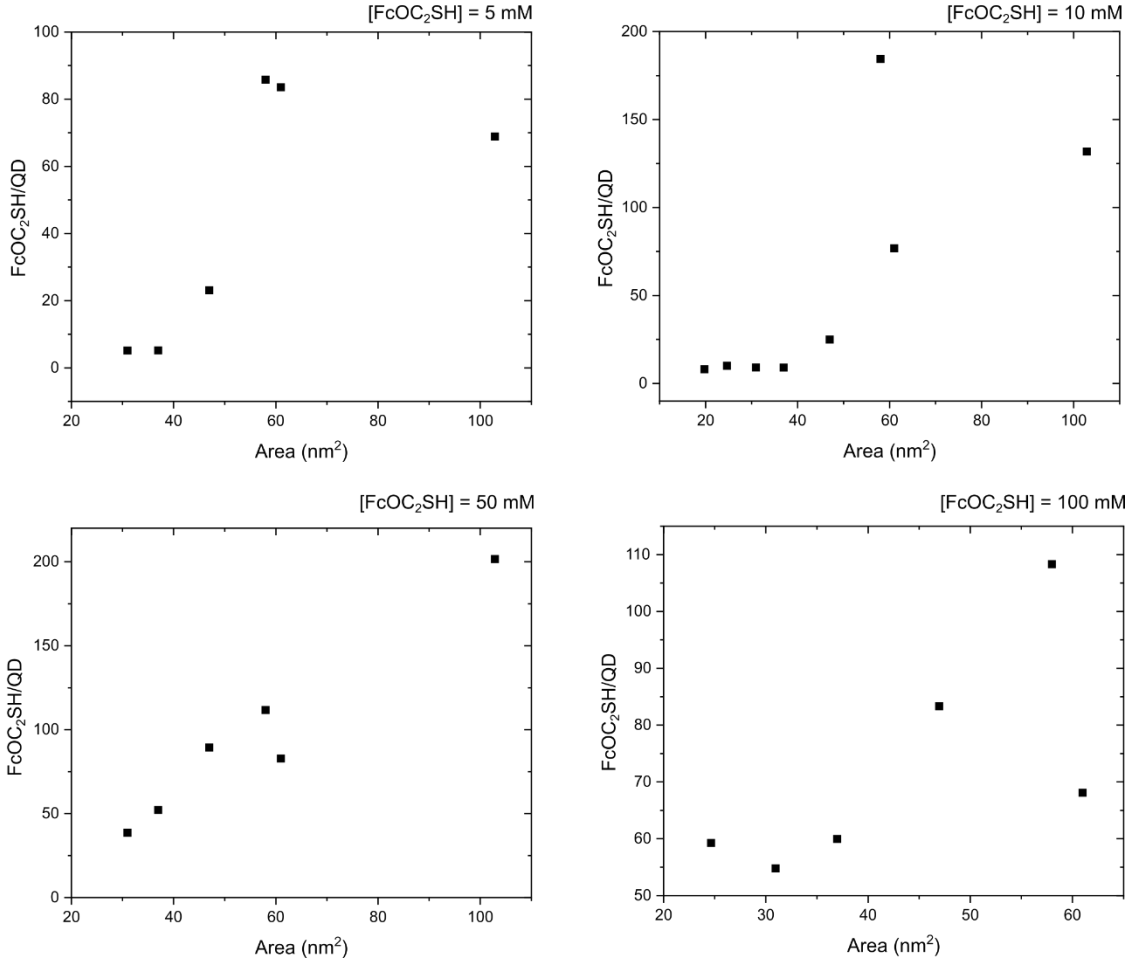

Figure S5. Variation of the number of $FcOC_2SH$ per QD ($FcOC_2SH$/QD) with the QD surface area for different concentrations of $FcOC_2SH$ during ligand exchange ([$FcOC_2SH$], shown as an inset on top of each graph). The surface area was determined assuming the QD are perfect spheres using the diameter determined by TEM.

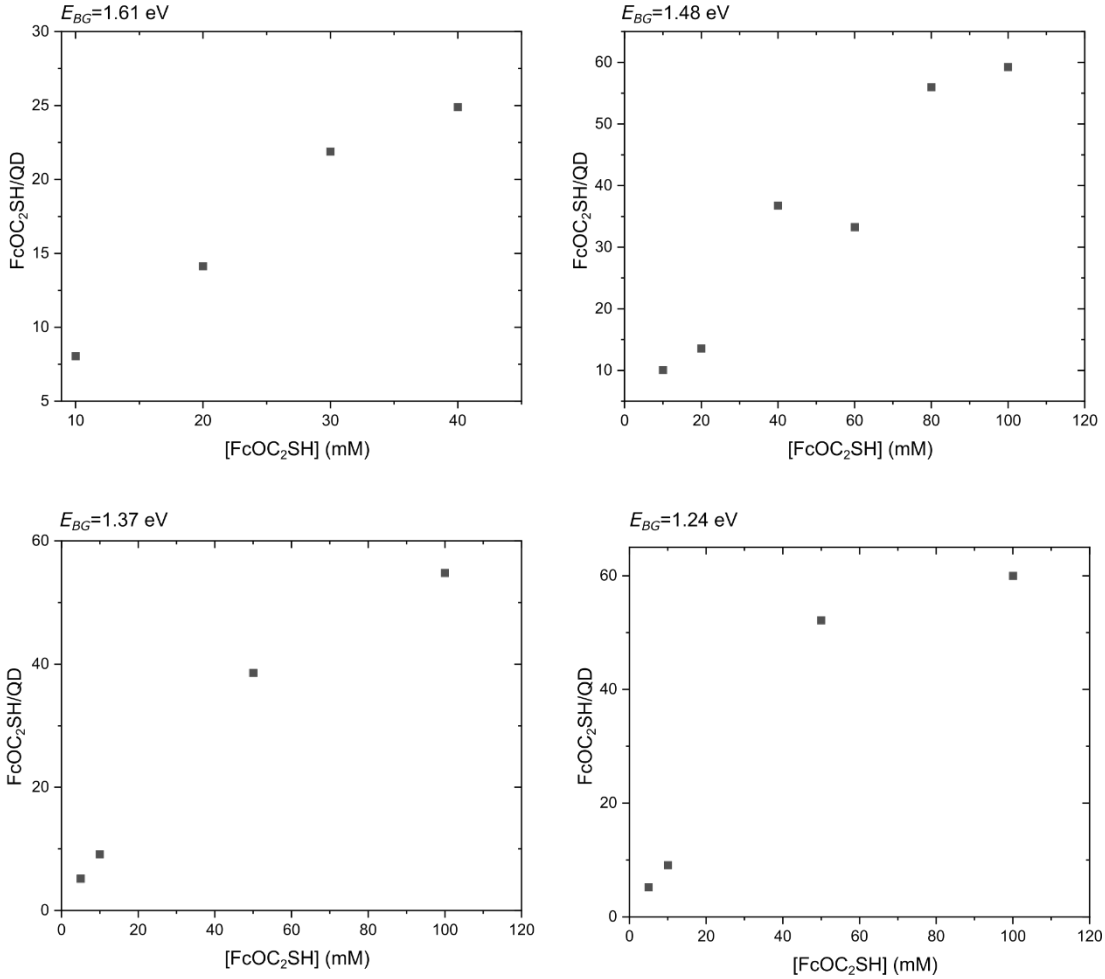

Figure S6. Variation of the number of $FcOC_2SH$ per QD ($FcOC_2SH$/QD) with the concentration of $FcOC_2SH$ used during ligand exchange ([$FcOC_2SH$]) for PbS-$FcOC_2SH$ QDs with different bandgaps (E_{BG}, shown as an inset on top of each graph).

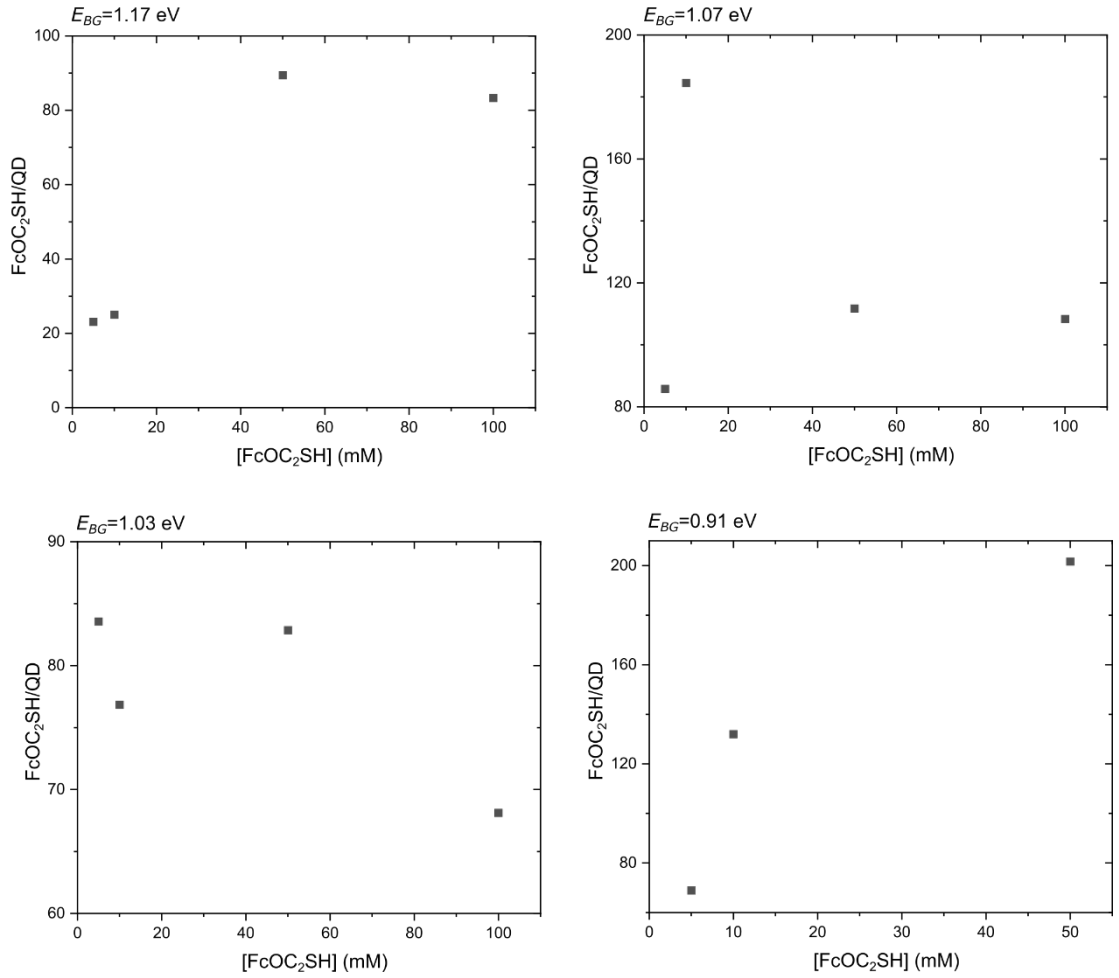

Figure S7. Variation of the number of $FcOC_2SH$ per QD ($FcOC_2SH$/QD) with the concentration of $FcOC_2SH$ used during ligand exchange ([$FcOC_2SH$]) for PbS-$FcOC_2SH$ QDs with different bandgaps (E_{BG}, shown as an inset on top of each graph).

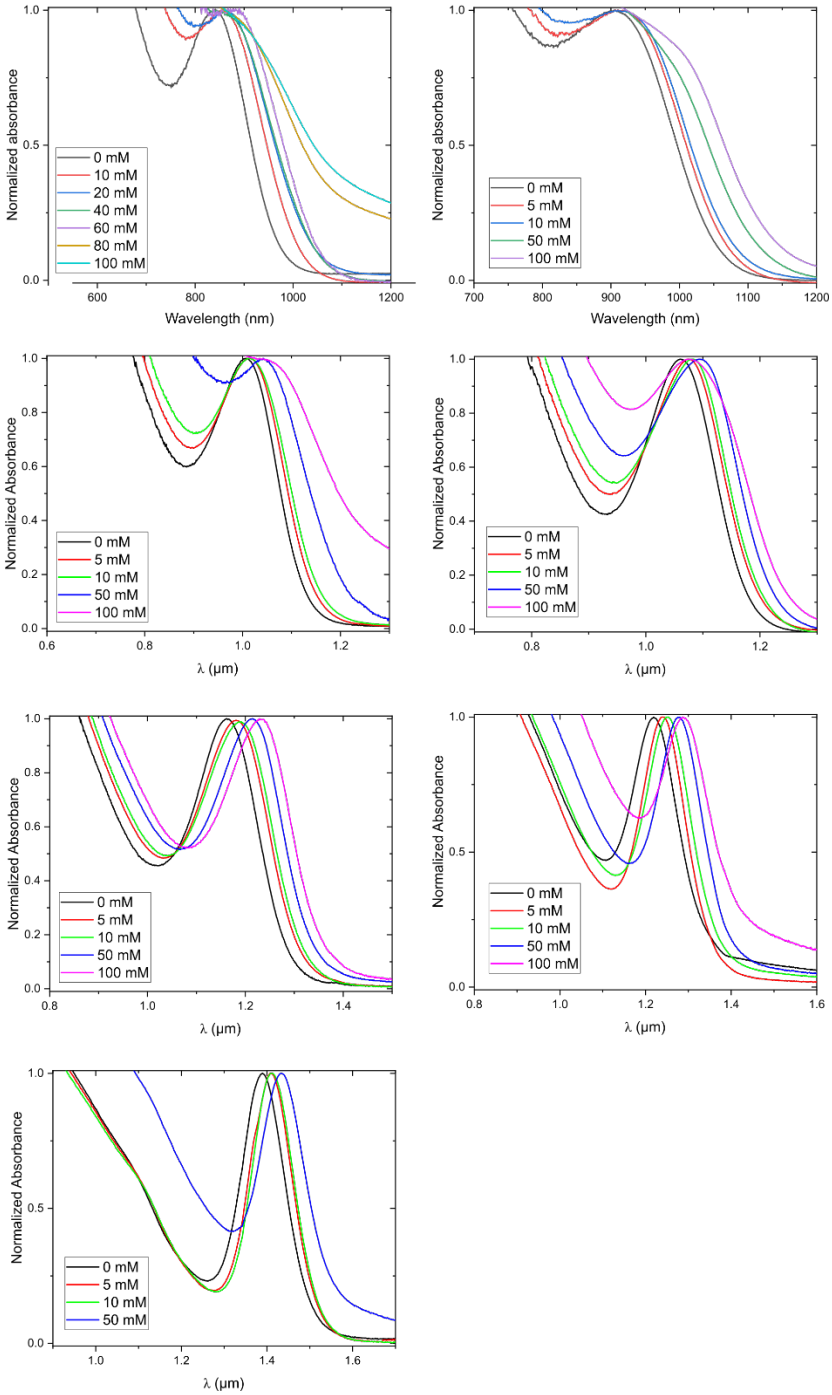

Figure S8. Steady-state absorption spectra of PbS and PbS-$FcOC_2SH$ as a function of the concentration of $FcOC_2SH$ used during ligand exchange (indicated in the inset) for QDs with different diameters. The 1Se1Sh peak shifts to the red and broadens with increasing concentration of $FcOC_2SH$ ligands. The broadening is more pronounced for smaller QDs, and the red shift is more pronounced for larger particles.

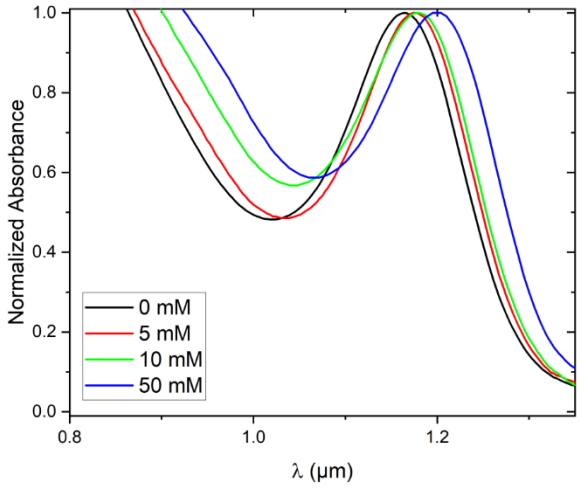

Figure S9. Steady-state absorption spectra of PbS and PbS-C_8SH as a function of the concentration of C_8SH used during ligand exchange (indicated in the inset).

S5: Average number of excitons per QD

The average excitons per QD, <N>, was calculated using two independent methods. Both methods give values of <N> that agree within a factor of two. For all experiments <N> was kept below 0.1.

The first method for determining <N> uses the excitation fluence (J) and the absorption cross section (σ):

$$< N >= J\sigma \quad \text{(S17)}$$

For PbS QDs of radius r, σ is given by the following empirical formula:[5]

$$\sigma = 7.494 \times 10^{-17} r^{2.31} \quad \text{(S18)}$$

The second method uses the 1S absorption bleach fraction ($\Delta A/ A_0$):

$$< N >= \frac{\Delta A}{A_0} g \quad \text{(S19)}$$

Where g is the 1S degeneracy (g=4 for PbS QDs).

The probability of a QD to have N excitons (P_N) was found from Poisson statistics:

$$P_N = \frac{<N>^N \times e^{<N>}}{N!} \quad \text{(S20)}$$

Which gives a probability of <1% for N=2 for all experiments.

S6: Charge carrier dynamics of PbS and PbS-$FcOC_2SH$

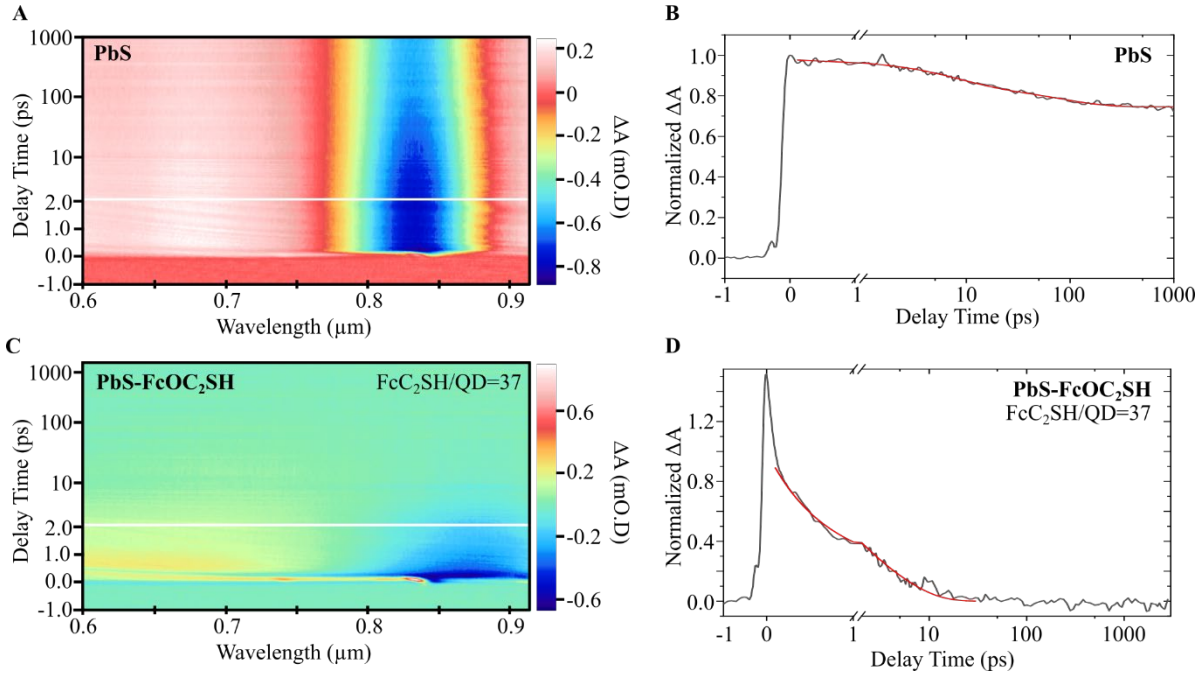

Figure S10. Transient absorption spectra and time decays of **(A,B)** PbS and **(C,D)** PbS-$FcOC_2SH$ with a bandgap of 1.47 eV, and with $FcOC_2SH$/QD = 37 for the later. In (B,D) the black line is the experimental data and the red line a biexponential fit.

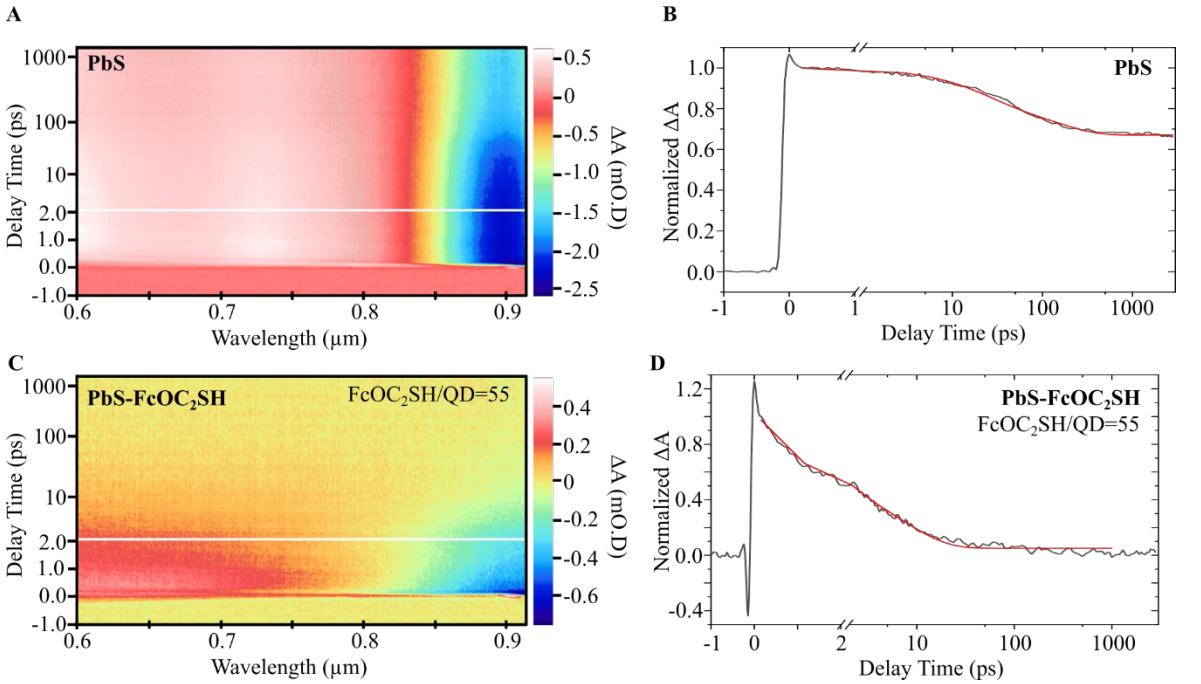

Figure S11. Transient absorption spectra and time decays of **(A,B)** PbS and **(C,D)** PbS-$FcOC_2SH$ with a bandgap of 1.37 eV, and with $FcOC_2SH$/QD = 55 for the later. In (B,D) the black line is the experimental data and the red line a biexponential fit.

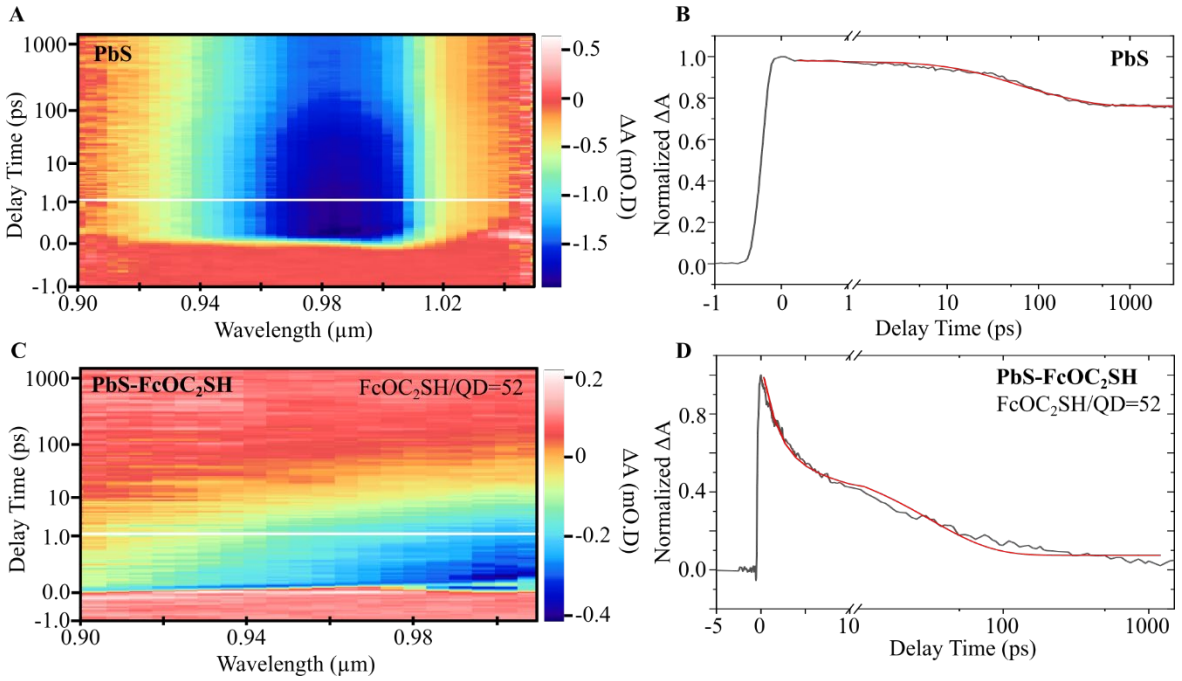

Figure S12. Transient absorption spectra and time decays of **(A,B)** PbS and **(C,D)** PbS-$FcOC_2SH$ with a bandgap of 1.23 eV, and with $FcOC_2SH$/QD = 52 for the later. In (B,D) the black line is the experimental data and the red line a biexponential fit.

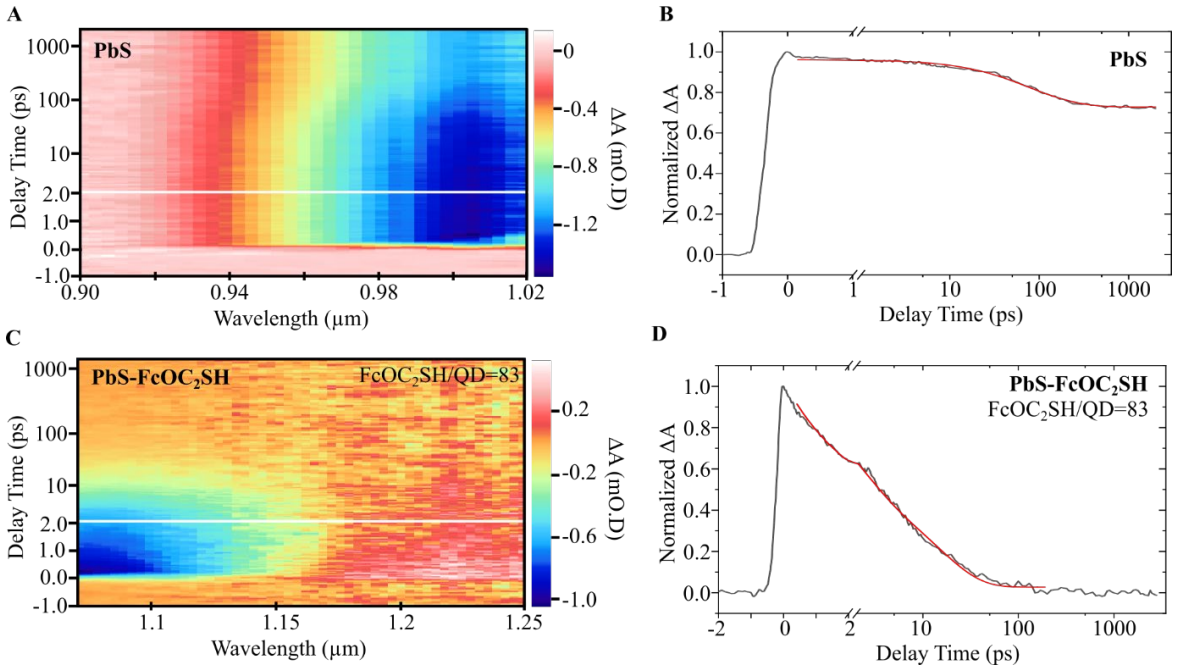

Figure S13. Transient absorption spectra and time decays of **(A,B)** PbS and **(C,D)** PbS-$FcOC_2SH$ with a bandgap of 1.17 eV, and with $FcOC_2SH$/QD = 83 for the later. In (B,D) the black line is the experimental data and the red line a biexponential fit.

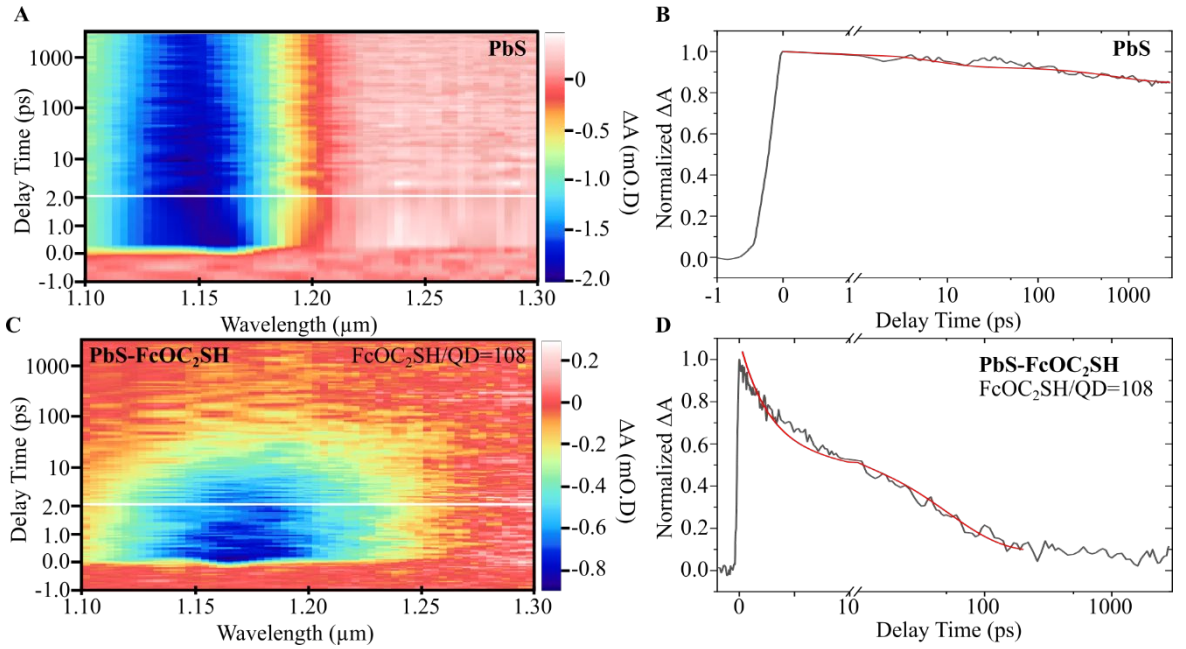

Figure S14. Transient absorption spectra and time decays of **(A,B)** PbS and **(C,D)** PbS-$FcOC_2SH$ with a bandgap of 1.07 eV, and with $FcOC_2SH$/QD = 108 for the later. In (B,D) the black line is the experimental data and the red line a biexponential fit.

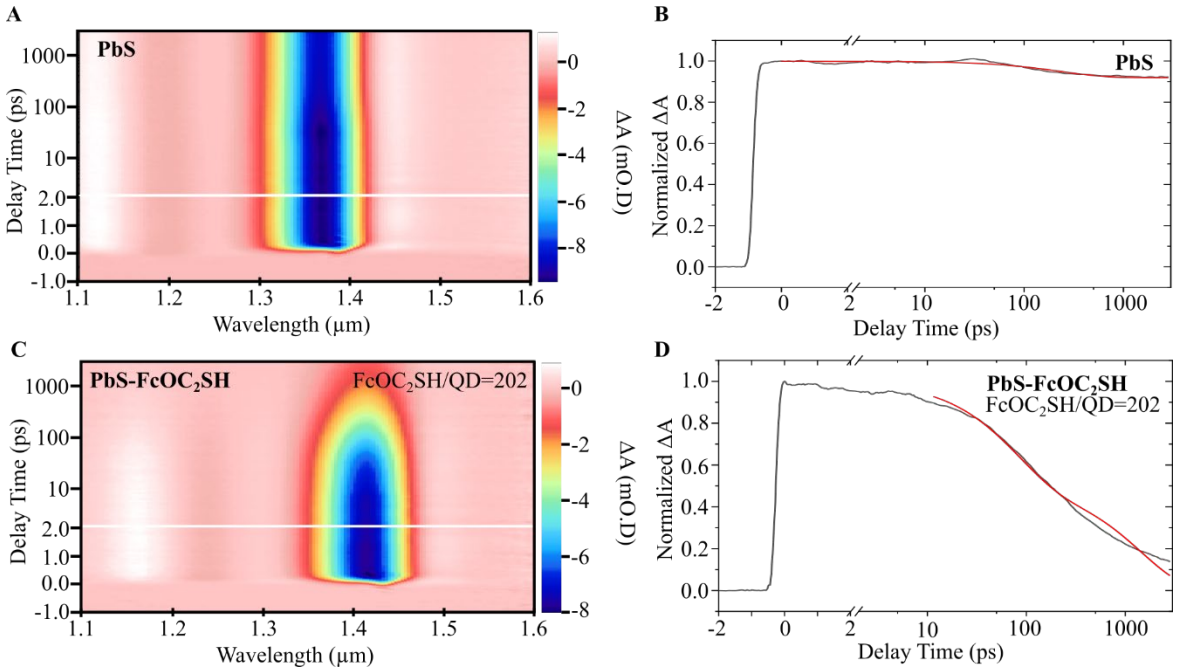

Figure S15. Transient absorption spectra and time decays of **(A,B)** PbS and **(C,D)** PbS-$FcOC_2SH$ with a bandgap of 0.89 eV, and with $FcOC_2SH$/QD = 202 for the later. In (B,D) the black line is the experimental data and the red line a biexponential fit.

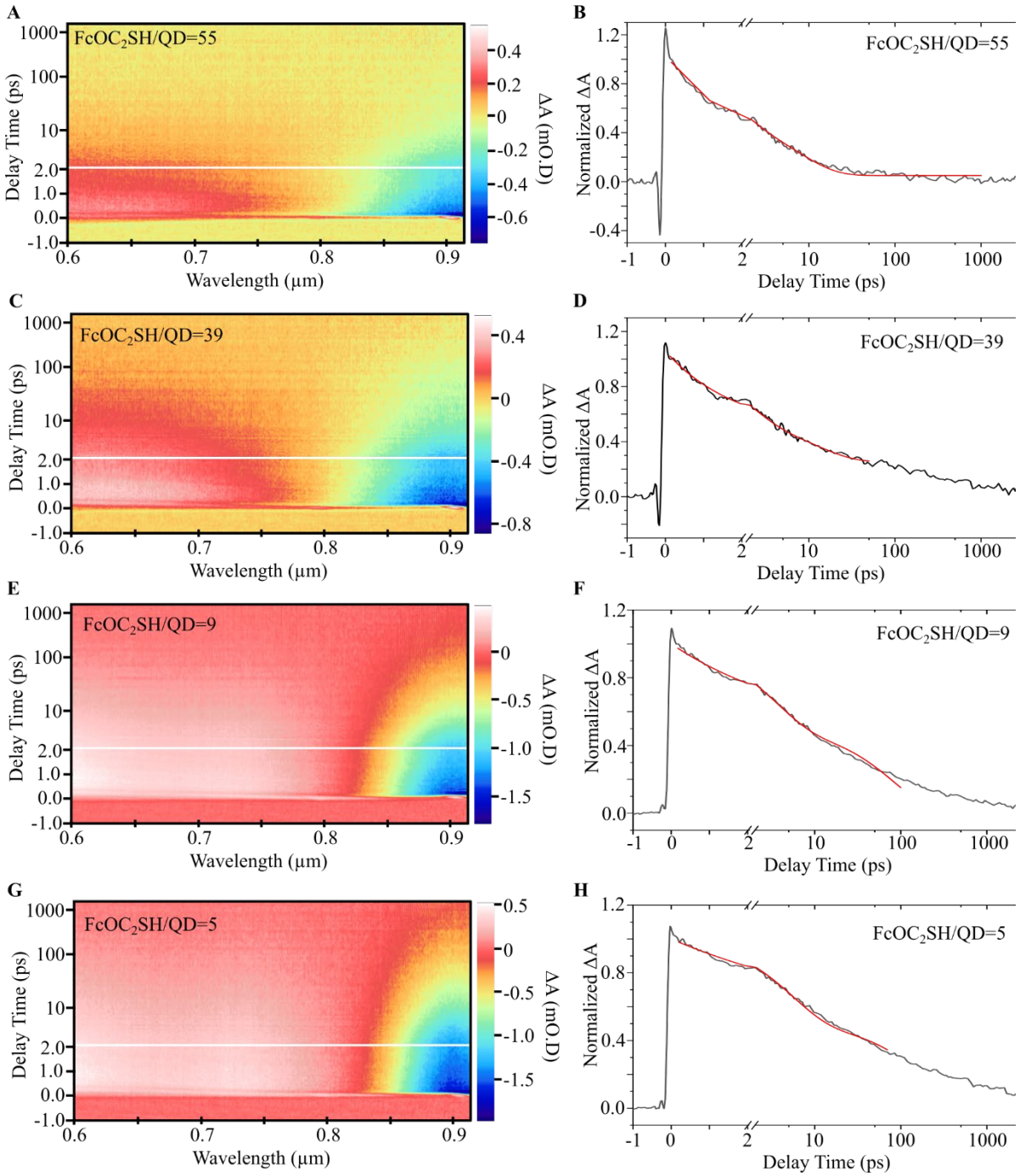

Figure S16. Transient absorption spectra and time decays as a function of $FcOC_2SH$/QD (indicated as an inset on each graph) for PbS-$FcOC_2SH$ with a bandgap of 1.47 eV. In (B,D,F,H) the black line is the experimental data and the red line a biexponential fit.

S7: Determination of the free energy of charge separation and charge recombination

We determined ΔG^0_{CS} and ΔG^0_{CR} from the values of k_{CS} and k_{CR} as a function of E_{BG} (Figure S24). The assumption we make here is that the value of λ and H_{AB} is the same for both CS and CR. Then we determined the energy level offset at which the CS and CR rate constants are equal for the same ΔG^0 value, *i.e.* $k_{CS}=k_{CR}$ for $\Delta G^0_{CS}=\Delta G^0_{CR}$. In practice, this was done by introducing an adjustable parameter x so that $\Delta G^0_{CS}=E_{BG}/2+x$ and $\Delta G^0_{CR}=E_{BG}/2-x$. x therefore represents the shift of the HOMO from mid-bandgap, and it is varied until $k_{CS}=k_{CR}$ for $\Delta G^0_{CS}=\Delta G^0_{CR}$. The factor 1/2 comes from the theoretical expectation that the $1S_e$ and $1S_h$ levels shift symmetrically with bandgap. However, experimentally is found that the $1S_e$ level shifts twice as much as the $1S_h$ level.[6, 7] This would result in a factor of 1/3 for CS and 2/3 for CR. We note that the condition $k_{CS}=k_{CR}$ for $\Delta G^0_{CS}=\Delta G^0_{CR}$ is satisfied better when we use a symmetrical shift of the $1S_e/1S_h$ levels (*i.e.*, a factor of ½) and therefore use those ΔG^0 values subsequently. Nevertheless, the conclusions we arrive do not depend on the values of ΔG^0, factor and/or x because the accessed *change* in ΔG^0 value is always higher than λ.

We next determine the absolute energy levels of the QDs CB and VB edges with knowledge of the HOMO level of $FcOC_2SH$, as determined by cyclic voltammetry (Figure S17) and ΔG^0_{CS} and ΔG^0_{CR}. The resulting alignment is shown in Figure 5A of the main text.

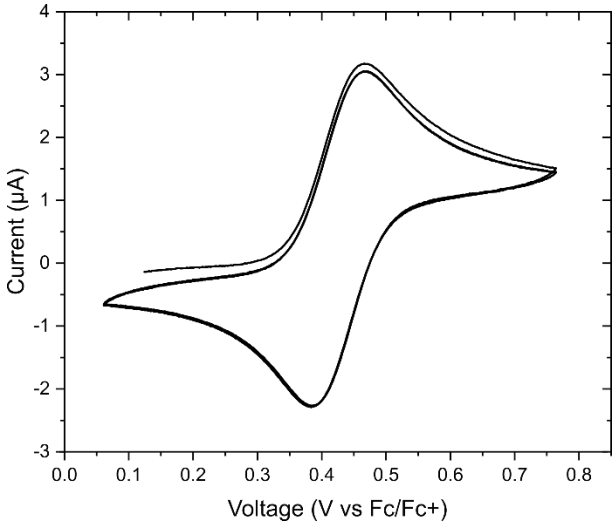

Figure S17. Cyclic voltammetry (50 mV/s) of $FcOC_2SH$ (1 mM) in 0.1 M of $LiClO_4$ in acetonitrile on a gold polycrystalline electrode. The peak-to-peak separation is 85 mV, close to the theoretical 59 mV. We therefore take the half-peak potential as the formal reduction potential, which corresponds to the HOMO level and is at 0.425 V *vs.* ferrocene/ferrocenium.

S8: Kinetic model for PbS

This section describes the theoretical model we developed based on a system of differential equations to describe the charge transfer kinetics of PbS. We also show that a biexponential fit (*Equation 2* in the main text) gives similar values as the model described here (Figure S18).

We obtained the trapping and trap recombination pseudo first order rate constants (k'_t and k'_{tr}, respectively), and fraction of QDs with traps (f), by fitting the TA decays with this model. For the fittings, we fixed the radiative pseudo first order rate constant k'_{rad} obtained from PL lifetime measurements (Figure S20).

The model assumes the presence of two QD populations: one without traps and another with traps, referred as A and B, respectively. The differential equations describing the charge dynamics of both populations are:

$$\frac{d[X]_A}{dt} = -k'_{rad}[X]_A \quad \text{(S21)}$$

$$\frac{d[X]_B}{dt} = -k'_{rad}[X]_B - k'_t[X]_B \quad \text{(S22)}$$

$$\frac{d[Xt]}{dt} = k'_t[Xt] - k'_{tr}[Xt] \quad \text{(S23)}$$

$$[X] = [X]_A + [X]_B \quad \text{(S24)}$$

Where $[X]_A$, $[X]_B$ and $[Xt]$ are the concentration of the excited state for particles A and B, and the trapped state concentration, respectively.

$[X]$ and $[Xt]$ are related to the normalized change in absorbance ΔA_{norm} through:

$$\Delta A_{norm} = [X] + \frac{[Xt]}{2} \quad \text{(S25)}$$

In the limit where $k'_t >> k'_{tr} >>> k'_{rad}$ the differential equations can be treated and solved independently, giving an analytical solution in the form of a sum of two exponential functions that englobe charge trapping and trap recombination, and a constant function that englobes the very long-lived radiative recombination:

$$\Delta A_{norm} = \frac{f}{2}e^{-k't t} + \frac{f}{2}e^{-k'tr t} + (1-f) \quad \text{(S26)}$$

For the fittings only f, k'_t and k'_{tr} were kept as variables. Figure S18 shows a comparison of these values obtained using the model (black squares) and the biexponential function (*equation S26*, red circles) as a function of the bandgap. Overall, both fittings converge into similar values, but where they do not, we used the full model to obtain the parameters as this should give more reliable results.

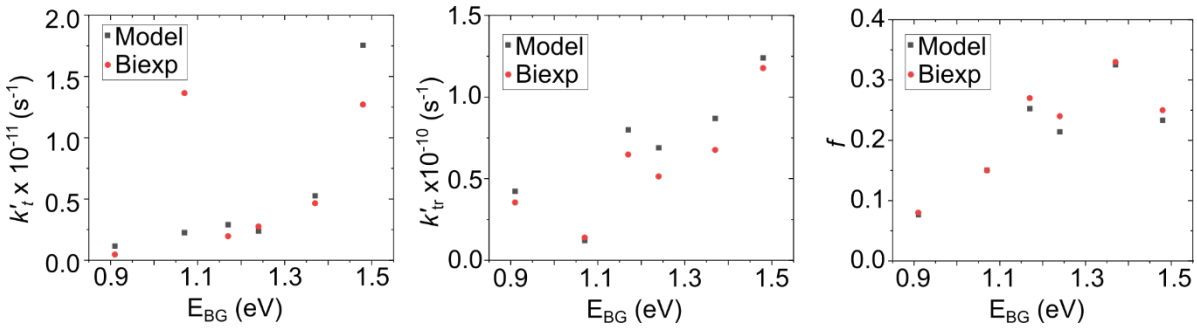

Figure S18. Comparison of the values of k'_t (left), k'_{tr} (center) and f (right) obtained using the model (black squares) and the biexponential function (red circles) as a function of the bandgap.

S9: Kinetic model for PbS-FcOC$_2$SH

This section describes the theoretical model we developed based on a system of differential equations to describe the charge transfer kinetics of PbS-FcOC$_2$SH. We also show that a biexponential fit (*Equation 3* of the main text) gives similar values as this model (Figure S19). We obtained the charge separation and recombination pseudo first order rate constants (k'_{CS} and k'_{CR}, respectively) by fitting the TA decays using this model.

This model assumes two populations of QDs: without traps and with traps, referred as C and D, respectively. The equations describing the charge dynamics of both populations are:

$$\frac{d[X]_C}{dt} = -k'_{rad}[X]_C - k'_{CS}[X] \quad \text{(S27)}$$

$$\frac{d[X-]_C}{dt} = k'_{CS}[X-]_C - k'_{CR}[X-]_C \quad \text{(S28)}$$

$$\frac{d[X]_D}{dt} = -k'_{rad}[X]_D - k'_{t}[X]_D - k'_{CS}[X]_D \quad \text{(S29)}$$

$$\frac{d[X-]_D}{dt} = k'_{CS}[X-]_D - k'_{CR}[X-]_D \quad \text{(S30)}$$

$$\frac{d[Xt]}{dt} = k'_{t}[Xt] - k'_{tr}[Xt] \quad \text{(S31)}$$

$$[X] = [X]_C + [X]_D \quad \text{(S32)}$$

$$[X-] = [X-]_C + [X-]_D \quad \text{(S33)}$$

Where $[X]_C$ and $[X]_D$ are the concentration of the excited state for particles C and D, respectively. $[X-]_C$ and $[X-]_D$ are the concentration of the charge separated state for particles C and D, respectively. $[Xt]$ is the trapped state concentration.

$[X]$, $[X-]$ and $[Xt]$ are related to the normalized change in absorbance ΔA_{norm} through:

$$\Delta A_{norm} = [X] + \frac{[X-]}{2} + \frac{[Xt]}{2} \quad \text{(S34)}$$

For the fittings only k'_{CS} and k'_{CR} were kept as variables, while f, k'_t and k'_{tr} were given the values obtained from the fitting of PbS without FcOC$_2$SH using the model described in Section S8.

In the limit where $k'_{rad} <<< k'_t$, $k'_{tr} << k'_{CS}$, k'_{CR}, the whole process can be described by a bi-exponential function:

$$\Delta A_{norm} = \frac{1}{2}e^{-k'_{CS}t} + \frac{1}{2}e^{-k'_{CR}t} \quad \text{(S35)}$$

Figure S19 shows a comparison of k'_{CS} and k'_{CR} obtained using the model (black squares) and the biexponential function (red circles) as a function of [FcOC$_2$SH] and bandgap.

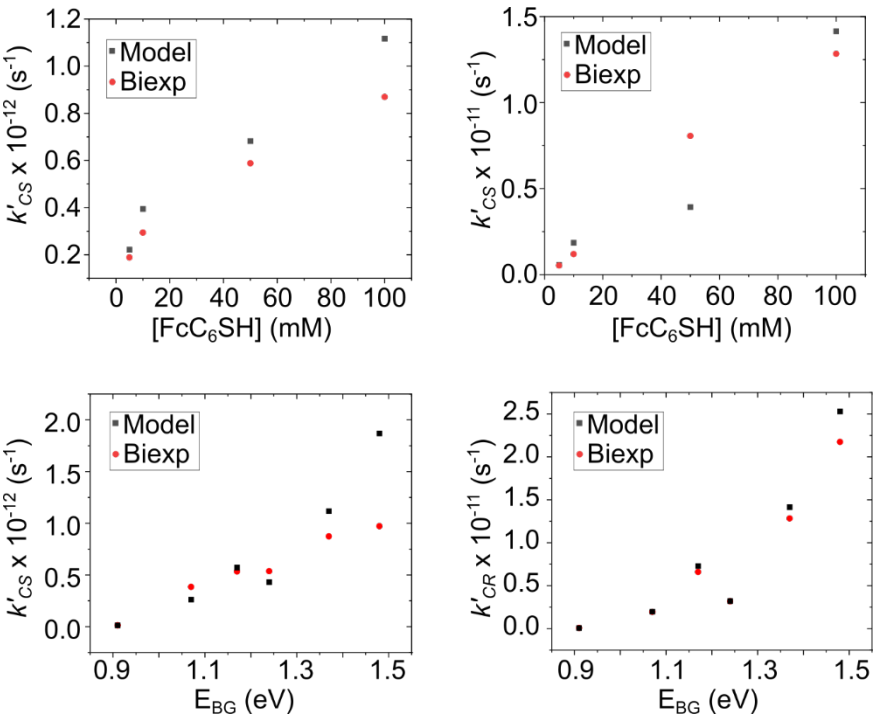

Figure S19. Comparison of the values of k'_{CS} (left) and k'_{CR} (right) obtained using the model (black squares) and the biexponential function (red circles) as a function of [$FcOC_2SH$] (top) and bandgap (bottom).

S10: Determination of PL, radiative and nonradiative rates

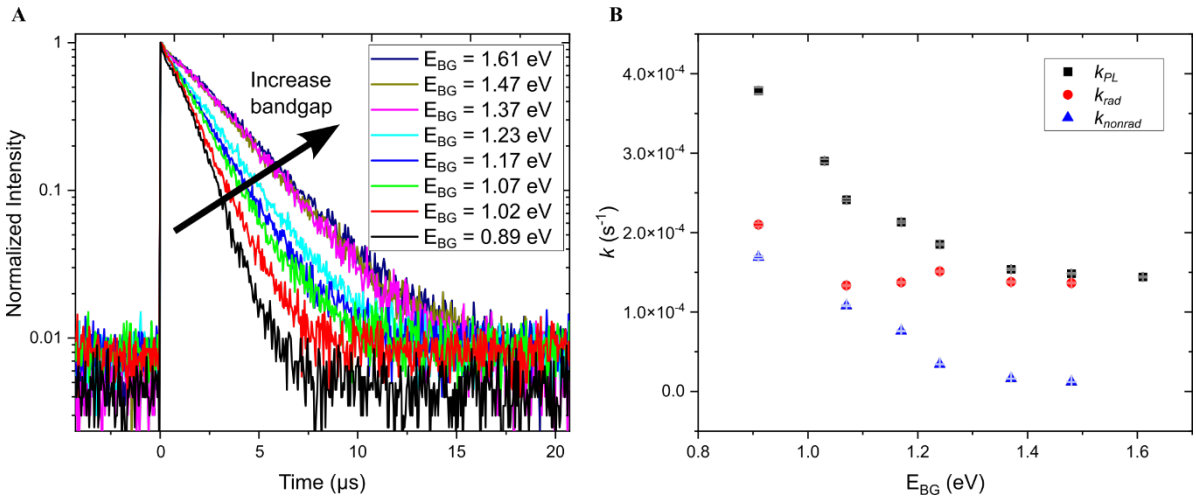

Figure S20. (A) Time resolved photoluminescence decays of PbS QDs as a function of the bandgap (indicated in the inset). **(B)** Rate constants (*k)* of photoluminescence decay (k_{PL}, black squares), radiative decay (k_{rad}, red circles) and nonradiative decay (k_{nonrad}, blue triangles) as a function of the bandgap for PbS QDs. k_{PL} was obtained from a monoexponential fit of the PL decays in (A), $k_{rad} = k_{PL}$ x PLQY / (1-f), and $k_{nonrad} = k_{PL} - k_{rad}$.

S11: Comparison of PLQY with TA data of PbS

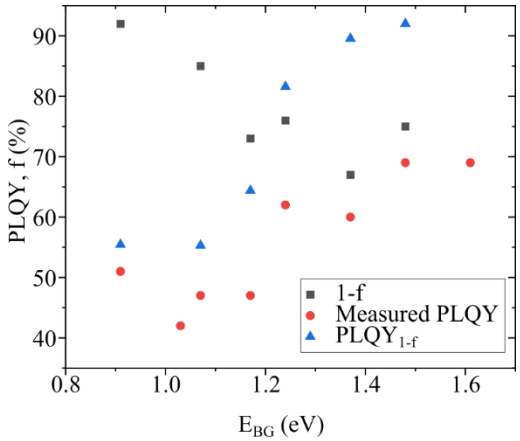

Figure S21. Measured photoluminescence quantum yield (PLQY, red circles), PLQY of QDs w/o traps ($PLQY_{1\text{-}ft}$ = PLQY/(1-*f*), blue triangles) and fraction of QDs without traps (1-f) as a function of bandgap energy for PbS QDs.

S12: Influence of linker length for charge transfer

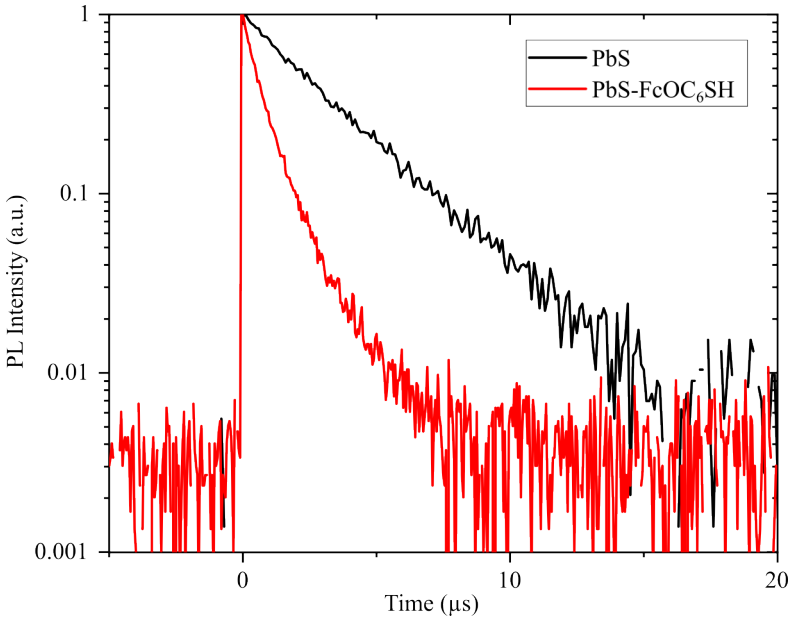

Figure S22. Time resolved photoluminescence decays of PbS QDs (black line) and PbS-$FcOC_6SH$ QDs (red line) with a bandgap of 1.55 eV dispersed in hexane.

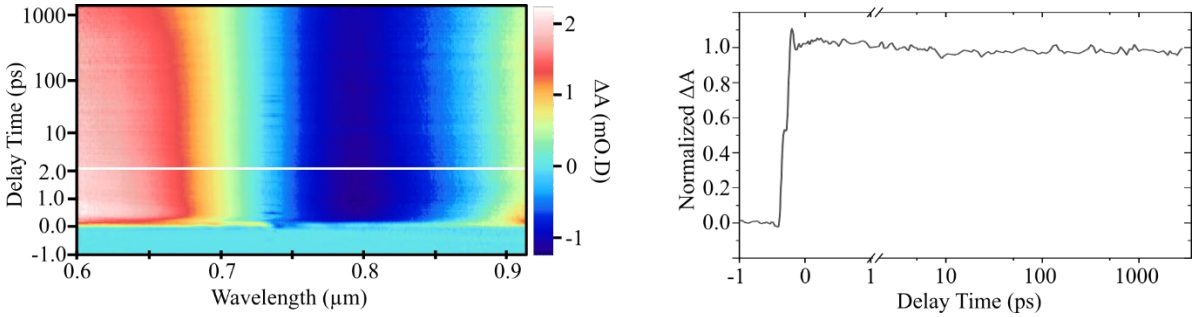

Figure S23. Transient absorption spectra and the band-edge time decay for PbS-$FcOC_6SH$ QDs with a bandgap of 1.55 eV dispersed in hexane.

S13: Rate constants of CS and CR as a function of bandgap

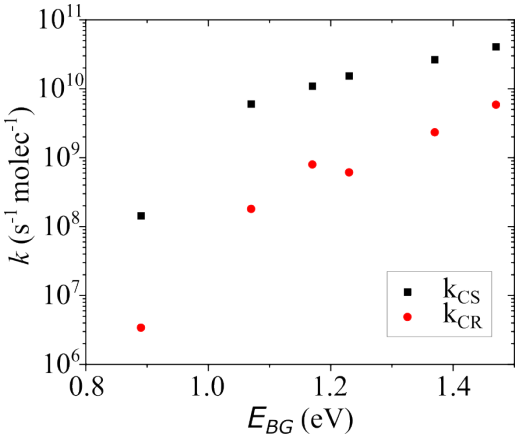

Figure S24. Experimentally measured rate constants for CS (black squares) and CR (red circles) as a function of the QD bandgap.

S14: Rate constants of CS and CR as a function of temperature

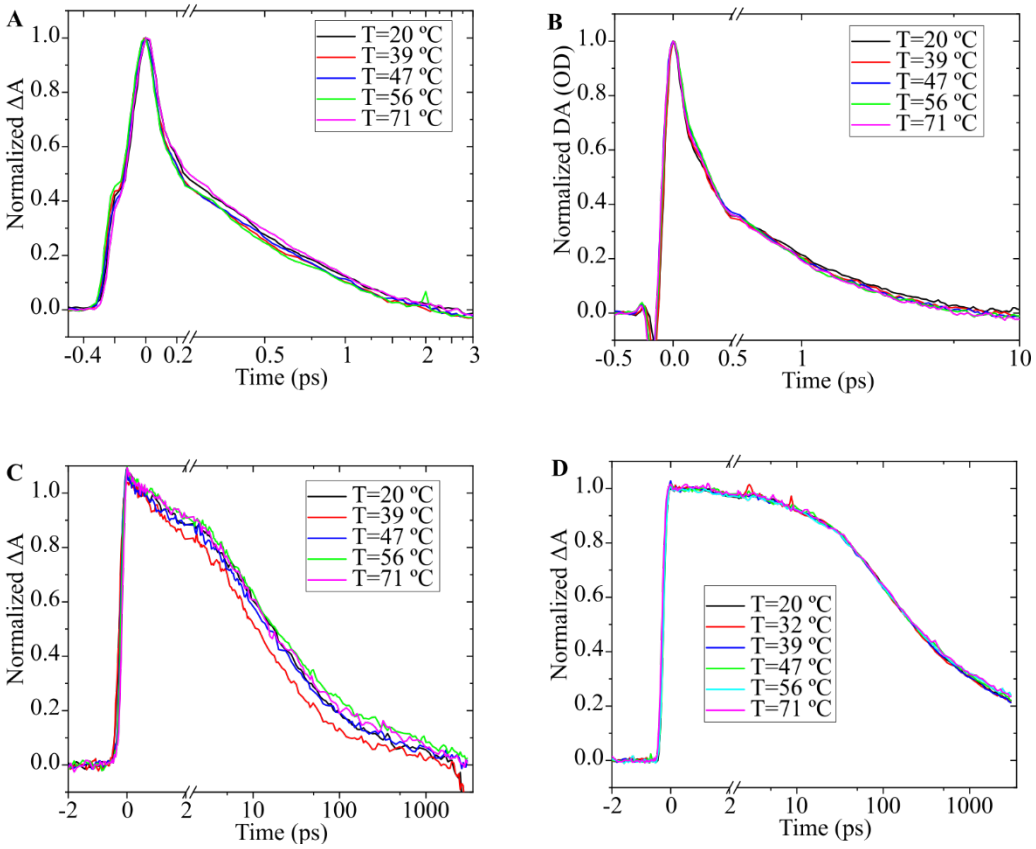

Figure S25. Transient absorption spectroscopy time decays at the band-edge of PbS-$FcOC_2SH$ as a function of temperature (indicated in the inset) with a bandgap of **(A)** 1.47 eV, **(B)** 1.37 eV, **(C)** 1.07 eV, and **(D)** 0.89 eV.

S15: References

(1) Paul, A.; Borrelli, R.; Bouyanfif, H.; Gottis, S.; Sauvage, F. Tunable Redox Potential, Optical Properties, and Enhanced Stability of Modified Ferrocene-Based Complexes. *ACS Omega* **2019**, *4* (12), 14780-14789. DOI: 10.1021/acsomega.9b01341 From NLM.
(2) Yazdani, N.; Andermatt, S.; Yarema, M.; Farto, V.; Bani-Hashemian, M. H.; Volk, S.; Lin, W. M. M.; Yarema, O.; Luisier, M.; Wood, V. Charge transport in semiconductors assembled from nanocrystal quantum dots. *Nature Communications* **2020**, *11* (1), 2852. DOI: 10.1038/s41467-020-16560-7.
(3) Dean, J. A. Lange's Handbook of Chemistry. McGraw-Hill: 1999.
(4) Seibold, E.; Sutton, L. Structure of ferrocene. *The Journal of Chemical Physics* **1955**, *23* (10), 1967-1967.
(5) Cademartiri, L.; Montanari, E.; Calestani, G.; Migliori, A.; Guagliardi, A.; Ozin, G. A. Size-Dependent Extinction Coefficients of PbS Quantum Dots. *Journal of the American Chemical Society* **2006**, *128* (31), 10337-10346. DOI: 10.1021/ja063166u.
(6) Vogel, Y. B.; Pham, L. N.; Stam, M.; Ubbink, R. F.; Coote, M. L.; Houtepen, A. J. Solvation Shifts the Band-Edge Position of Colloidal Quantum Dots by Nearly 1 eV. *Journal of the American Chemical Society* **2024**, *146* (14), 9928-9938. DOI: 10.1021/jacs.4c00402.
(7) Jasieniak, J.; Califano, M.; Watkins, S. E. Size-Dependent Valence and Conduction Band-Edge Energies of Semiconductor Nanocrystals. *ACS Nano* **2011**, *5* (7), 5888-5902. DOI: 10.1021/nn201681s.